



Electrical and structural properties of Mg-doped $\text{In}_x\text{Ga}_{1-x}\text{N}$ ($x \leq 0.1$) and p -InGaN/ n -GaN junction diode made all by RF reactive sputtering

Dong-Hau Kuo ^{*}, Thi Tran Anh Tuan, Cheng-Che Li, Wei-Chun Yen

Department of Materials Science and Engineering, National Taiwan University of Science and Technology, Taipei 10607, Taiwan



ARTICLE INFO

Article history:

Received 5 July 2014

Received in revised form 11 October 2014

Accepted 5 November 2014

Keywords:

Mg-In_xGa_{1-x}N films

p-n diode

Barrier height

Cheung's and Nodre methods

ABSTRACT

Mg-doped In_xGa_{1-x}N ($x = 0.025, 0.05, 0.075$, and 0.1) films have been deposited on Si (100) substrates by RF reactive sputtering. Mg-In_xGa_{1-x}N films remained *p*-type conduction at $x \leq 0.075$. This is the first try to have *p*-InGaN by sputtering. The film transformed into *n*-type conduction at $x = 0.1$. The highest mobility was found to be $62 \text{ cm}^2 \text{ V}^{-1} \text{ s}^{-1}$ in the Mg-In_{0.025}Ga_{0.975}N film, meanwhile the highest conductivity was found to be 9.1 S cm^{-1} in the Mg-In_{0.075}Ga_{0.925}N film due to the high hole concentration of $7.4 \times 10^{18} \text{ cm}^{-3}$. In addition, we also made *p-n* (*p*-Mg-In_{0.05}Ga_{0.95}N/*n*-GaN) junction diode all by using RF reactive sputtering. The *p-n* junction diode has leakage current of $2.7 \times 10^{-6} \text{ A}$, the turn-on voltage of $\sim 1.8 \text{ V}$, and the breakdown voltage $> -6.8 \text{ V}$. The *p-n* diode also has stable performance at elevated temperature.

© 2014 Published by Elsevier B.V.

1. Introduction

The creation of *p*-type GaN and InGaN materials has brought promising future for the application of optoelectronic and electronic devices. The success of Mg doping in forming *p*-type GaN and InGaN films is one of the important technology for developing LEDs or power effect devices [1–5]. In general, high hole concentration of *p*-layer has important role to improve electronic devices in reducing the leakage currents, threshold voltages, and increasing the breakdown voltages [6–8]. Lee et al. [2] found that high hole concentration of $1.6 \times 10^{18} \text{ cm}^{-3}$ was achieved for *p*-doped GaN:Mg layers grown at 1040°C by MOCVD for green LEDs. In the case of *p*-In_{0.04}Ga_{0.96}:Mg grown at 840°C , the hole concentration had a significant improvement due to the reduced ionization activation energy of Mg acceptors in InGaN. Chang et al. [3] successfully fabricated nitride-based LEDs with Mg-doped In_{0.23}Ga_{0.77}N capping layer. There was a decrease in the operation voltage from 3.78 to 3.37 V due to the introduction of a 5-nm-thick *p*-In_{0.23}Ga_{0.77}N layer on top of *p*-GaN layer. Ager et al. [4] reported that the high hole concentration of Mg-doped In_xGa_{1-x}N (with $x = 0.19$) were $6 \times 10^{19} \text{ cm}^{-3}$ by using capacitor–voltage (*C-V*) experiments. Chi et al. [5] considered that the Mg-diffused GaN films made by MOCVD had become *p*-type conductivity with hole concentration of $\sim 10^{17} \text{ cm}^{-3}$ and mobility of $10 \text{ cm}^2 \text{ V}^{-1} \text{ s}^{-1}$. K. Kumakura et al. [6] reported the electrical properties of Mg-In_xGa_{1-x}N ($x < 0.2$) grown

by metal-organic vapor phase epitaxy. The hole concentrations of Mg-doped In_{0.04}Ga_{0.96}N and In_{0.14}Ga_{0.86}N were $1.2 \times 10^{18} \text{ cm}^{-3}$ and $6.7 \times 10^{18} \text{ cm}^{-3}$, respectively, while it was $3.0 \times 10^{18} \text{ cm}^{-3}$ for Mg-GaN. At these days, *p*-type Mg-InGaN films are all made by MOCVD at $> 800^\circ\text{C}$. Low temperature process below 500°C has not been reported for *p*-type Mg-InGaN.

For investigation in the electric devices, Dupuis et al. [9] reported the electrical properties of In_{0.19}Ga_{0.81}N/GaN and In_{0.25}Ga_{0.75}N/GaN multiple quantum well (MQW) with different *p*-layers. The optical and structural properties of the MQW in LEDs were improved by reducing the growth temperature of the *p*-type layers. Cao et al. [10] reported the fabrication of *n*⁺–*p* junction by implantation of ²⁹Si⁺. The breakdown voltage, turn-on voltage, and ideality factor were -13 V , 5 V , and 2 , respectively. Lee et al. [11] studied the effect of *p*-GaN layers on the turn-on voltage of LEDs. The turn-on voltages at the forward bias were found in range of 5.5–6.5 V. Liu et al. [12] investigated the InGaN-based LEDs with a *p-n* GaN homojunction. The ideality factor was estimated to be 2.11 at voltage regime of 2 V and barrier height was determined to be 0.77 eV at the room temperature. Mohd Yusoff et al. [13] described the growth and characterization of *p-n* junction diodes based on GaN grown on Si(111) substrate. The extracted ideality factors had the range of 15.14–19.68, decreasing with an increase in testing temperature (30 – 104°C). The above-mentioned III-nitrides mainly used for LEDs have been fabricated by MOCVD above 800°C , while the low temperature process at and below 400°C has rarely been reported.

In our previous work, Mg doped *p*-GaN film (Mg $\sim 10.2\%$) have been successful deposited on Si (100) substrates by RF reactive

* Corresponding author. Tel.: +886 2 27303291; fax: +886 2 27303291.

E-mail address: dhkuo@mail.ntust.edu.tw (D.-H. Kuo).

sputtering technique [14]. We also fabricated a totally sputtering-made *p*-*n* GaN junction diode. In this study, we attempted to deposit *p*-type $\text{In}_x\text{Ga}_{1-x}\text{N}$ ($x = 0.025, 0.05, 0.075$, and 0.1) films by RF reactive sputtering with single Mg-containing cermet targets. Furthermore, to prove the success in making *p*-type InGaN films, we also made a *p*-*n* junction diode with the selections of GaN for the *n*-layer and Mg-doped $\text{In}_x\text{Ga}_{1-x}\text{N}$ for the *p*-layer. The electrical *I*-*V* characteristics of device were determined by thermionic emission (TE) mode at the wide testing temperature. The incentive of this work is originated from curiosity on how far this technology used for electronic devices instead of LEDs can achieve.

2. Experimental

Mg-doped $\text{In}_x\text{Ga}_{1-x}\text{N}$ films were deposited on Si (100) and transparent glass substrates by RF reactive sputtering for the purpose of different characterizations. The sputtering cermet targets were prepared by hot pressing the mixture of metallic In, Ga, and Mg powders and ceramic GaN powder. The $[\text{Mg}]/([\text{In}] + [\text{Ga}] + [\text{Mg}])$ molar ratio in each cermet target was kept at 15%. The $[\text{In}]/([\text{In}] + [\text{Ga}] + [\text{Mg}])$ molar ratios were 0.025, 0.05, 0.075, and 0.1. The chamber pressure was vented to 1×10^{-6} Torr by diffusion pump to avoid the oxygen and impurities before sputtering. The working distance between samples and targets in chamber was kept at 5 cm. The deposition temperature and working pressure were kept at 400°C and 9×10^{-3} Torr, respectively. The $\text{Mg}-\text{In}_x\text{Ga}_{1-x}\text{N}$ targets were sputtered under 150 W for 1 h while the flow rate of Ar and N₂ was kept at 5 sccm for each.

In addition, the *p*-*n* junction diode was made by RF reactive sputtering by selecting GaN for the *n*-layer and $\text{Mg-In}_{0.05}\text{Ga}_{0.95}\text{N}$ for the *p*-layer. The $p\text{-In}_{0.05}\text{Ga}_{0.95}\text{N}$ film was also deposited on Pt/TiO₂/Si substrate. After depositing $p\text{-In}_{0.05}\text{Ga}_{0.95}\text{N}$ film, the *n*-GaN film was grown at 200°C under RF power of 120 W for 40 min. The Al layer on the top was sputtered at 200°C for 30 min with a pure Al target. Only Ar gas was used at the flow rate of 5 sccm meanwhile the RF power was kept at 80 W. Pt and Al were the electrodes of *p*-*n* junction diode.

Crystalline phase and growth orientation of $\text{Mg-In}_x\text{Ga}_{1-x}\text{N}$ films were analyzed by X-ray diffraction (XRD, D8 Discover, Bruker). Scanning electron microscopy (SEM, JSM-6500F, JEOL) and atomic force microscopy (AFM, Dimension Icon, Bruker) were used to observe the surface morphology of $\text{Mg-In}_x\text{Ga}_{1-x}\text{N}$ films. Energy dispersive spectrometer (EDS, JSM-6500F, JEOL) equipped on SEM was used for composition analysis. The dual beam focused ion beam microscope (Quanta 3D FEG, FEI) with the ion beam source was used to prepare the cross-sectional TEM samples. The carrier concentration, electrical conductivity, and mobility were measured by Hall measurement (HMS-2000, Ecopia) at room temperature with the maximum magnetic field of 0.51 T. Ultraviolet–Visible (UV–vis) Spectrometer (V-670, Jasco) was used to measure the absorption spectra for $\text{Mg-In}_x\text{Ga}_{1-x}\text{N}$ films which were deposited on glass substrates. The electrical characteristics (*I*-*V*) of sputtering-made *p*-*n* junction diode were determined by Semiconductor Device Analyzer (Agilent, B1500A) in the temperature range of 25–150 °C.

3. Results and discussion

3.1. Structural and surface morphological characteristics

Table 1 shows the EDS results of $\text{Mg-In}_x\text{Ga}_{1-x}\text{N}$ films at $x = 0.025, 0.05, 0.075$, and 0.1 . The $[\text{N}]/([\text{In}] + [\text{Ga}] + [\text{Mg}])$ ratios were smaller than 1, which means that the deposited $\text{Mg-In}_x\text{Ga}_{1-x}\text{N}$ films by RF reactive sputtering are in a nitrogen-deficient state. As the Mg content in each $\text{Mg-In}_x\text{Ga}_{1-x}\text{N}$ target was kept at 15%, the $[\text{Mg}]/([\text{In}] + [\text{Ga}] + [\text{Mg}])$ ratios in films were 11.9, 12.7, 14.6, and

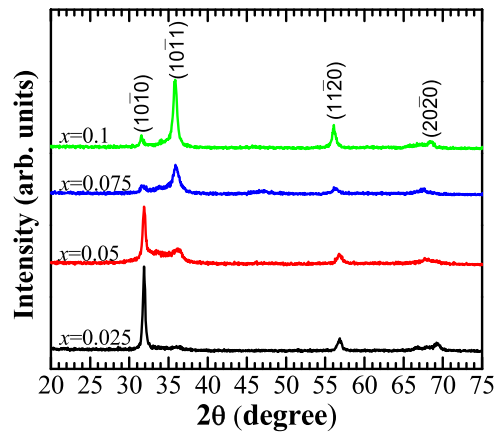


Fig. 1. XRD patterns of Mg-In_xGa_{1-x}N films ($x = 0.025, 0.05, 0.075$, and 0.1) deposited at 400°C on Si substrates in Ar/N₂ atmosphere with different indium contents in cermet targets.

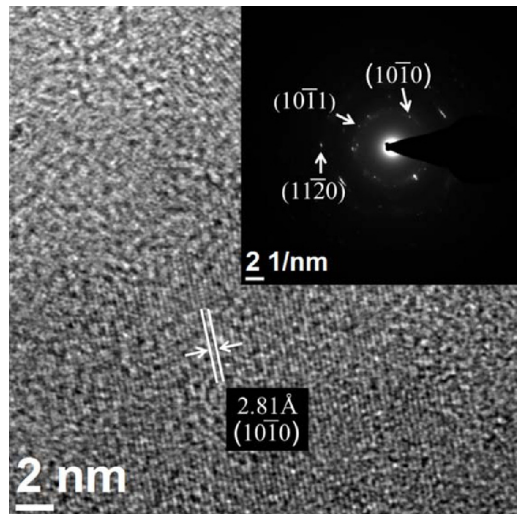
13.0 at.% at $x = 0.025, 0.05, 0.075$ and 0.1 , respectively. All the Mg contents in Mg-In_xGa_{1-x}N films decreased slightly compared with those in Mg-In_xGa_{1-x}N targets. The In element is expected to help the Mg atoms dissolve into the GaN lattice and form solid solution. However, the In content in Mg-In_{0.1}Ga_{0.9}N film increased to 16.2%, but its Mg content did not increase but slightly decreased to 13.0%, as compared to 14.6% for Mg-In_xGa_{1-x}N at $x = 0.075$. In this work, the In effect is not a strong factor for Mg solubility in InGaN.

Fig. 1 shows XRD patterns of the Mg-In_xGa_{1-x}N films. The XRD results indicated that all Mg-In_xGa_{1-x}N films deposited on Si (100) substrates had wurtzite structure and exhibited polycrystalline. With the SEM image shown later, the films under XRD tests had a thickness of 1.1 μm. For the Mg-In_{0.025}Ga_{0.975}N and Mg-In_{0.05}Ga_{0.95}N films, they showed the preferentially (10̄10)-oriented diffraction planes located at $2\theta = 31.9^\circ$. As the In content increased to 13.8 and 16.2% for Mg-In_{0.075}Ga_{0.925}N and Mg-In_{0.1}Ga_{0.9}N films, respectively, their preferential growth planes changed to the (10̄11) plane accompanied by a second diffraction peak from the (11̄20) plane due to the lattice distortion. Besides, our sputtered Mg-In_xGa_{1-x}N films do not show any phase separation or secondary phases. This means that the Mg dopant completely dissolves into In_xGa_{1-x}N by RF reactive sputtering, which forms solid solution or the Mg cation replaces the lattice site of the Ga cation. The *p*-Mg-In_xGa_{1-x}N films deposited on Pt/TiO₂/Si substrate also were analyzed by XRD. Basically, the peak intensity and position were all similar for those on Si substrates. The different substrates will have different nucleation and growth behaviors for the film growth and their morphology, composition, electrical property etc. all can have differences. Our sputtered III-nitride films had a fast growth rate of 27.5 nm/s and were polycrystalline, which minimized their differences in nucleation and growth behaviors.

The structure property of the Mg-In_{0.05}Ga_{0.95}N film was performed by using high-resolution TEM (HR-TEM). The *p*-Mg-In_{0.05}Ga_{0.95}N film was deposited by RF reactive sputtering on Pt/TiO₂/Si substrate at 400°C under 150 W for 40 min. Fig. 2 shows the TEM image of Mg-In_{0.05}Ga_{0.95}N film and the inset image shows the selected area electron diffraction (SAED) pattern of Mg-In_{0.05}Ga_{0.95}N film. The Mg-In_{0.05}Ga_{0.95}N film exhibited polycrystalline and the d-space value from the lattice fringe was calculated to be 2.81 Å, which corresponded to the (10̄10) crystalline plane. The SAED pattern also demonstrated the polycrystalline nature of Mg-InGaN. The (10̄10), (10̄11), and (11̄20) crystal planes were shown in the pattern, which were consistent with the XRD results. There are no precipitates observed by the HR-TEM in Fig. 2. The segregation of In and Mg can be excluded. The formation of solid solution is supported by this observation.

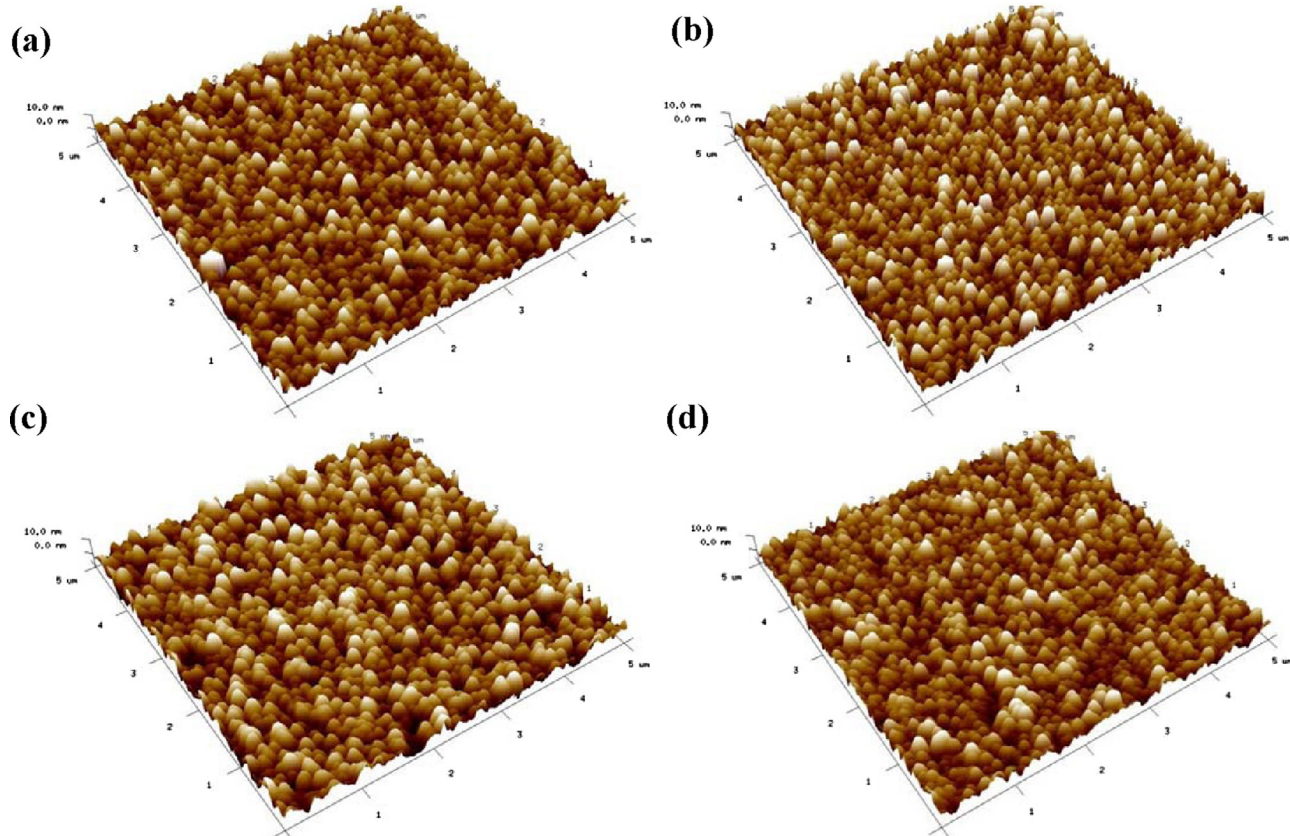
Table 1Compositional analyses of Mg-In_xGa_{1-x}N films at $x=0.025, 0.05, 0.075$, and 0.1 .

Mg-In _x Ga _{1-x} N films	In (at.%)	Ga (at.%)	Mg (at.%)	N (at.%)	[Mg]/([In]+[Ga]+[Mg])	[In]/([In]+[Ga]+[Mg])	[N]/([In]+[Ga]+[Mg])
$x=0.025$	2.73	42.43	6.12	48.72	0.119	0.053	0.950
$x=0.05$	3.79	44.33	7.01	44.86	0.127	0.069	0.814
$x=0.075$	8.09	42.00	8.59	41.33	0.146	0.138	0.704
$x=0.1$	9.30	40.64	7.43	42.63	0.130	0.162	0.743

**Fig. 2.** HRTEM image of Mg-In_{0.05}Ga_{0.95}N film deposited at 400 °C on a Si substrate in Ar/N₂ atmosphere. The inset shows the SEAD pattern of Mg-In_{0.05}Ga_{0.95}N film.

Surface morphologies of Mg-In_xGa_{1-x}N films were analyzed by AFM, as shown in Fig. 3. The root-mean-square (rms) roughness values were found to be 3.83, 3.67, 3.36, and 3.10 nm for Mg-In_xGa_{1-x}N films at $x=0.025$ (Fig. 3(a)), 0.05 (Fig. 3(b)), 0.075 (Fig. 3(c)), and 0.1, (Fig. 3(d)), respectively. The surface roughness could be improved by increasing the In content. In this work, the roughness is not a strong function of the Mg content, as its content is not largely changed. Our rms values were larger than the films grown by MOCVD with roughness of 0.6–1.1 nm [3,9]. Our Mg-In_xGa_{1-x}N films were rougher due to the lower deposition temperature of 400 °C. Low substrate temperature cannot provide sufficient kinetic energy for the adatoms to grow into epitaxial layer instead forming the polycrystalline films.

The carrier concentration, mobility, and electrical conductivity of Mg-In_xGa_{1-x}N films are shown in Fig. 4. As the In content increased to 5.3% for Mg-In_{0.025}Ga_{0.975}N film, the as-deposited film exhibited the p-type conduction without the need of thermal annealing. The hole concentration and mobility of Mg-In_{0.025}Ga_{0.975}N film were found to be $1.1 \times 10^{17} \text{ cm}^{-3}$ and $62 \text{ cm}^2 \text{ V}^{-1} \text{ s}^{-1}$, respectively. Furthermore, with increasing the In content to 6.9% of Mg-In_{0.05}Ga_{0.95}N film and 13.8% of Mg-In_{0.075}Ga_{0.925}N film, the hole concentration increased to 1.3×10^{17}

**Fig. 3.** AFM surface images of Mg-In_xGa_{1-x}N films at $x=(\text{a}) 0.025, (\text{b}) 0.05, (\text{c}) 0.075$, and $(\text{d}) 0.1$.

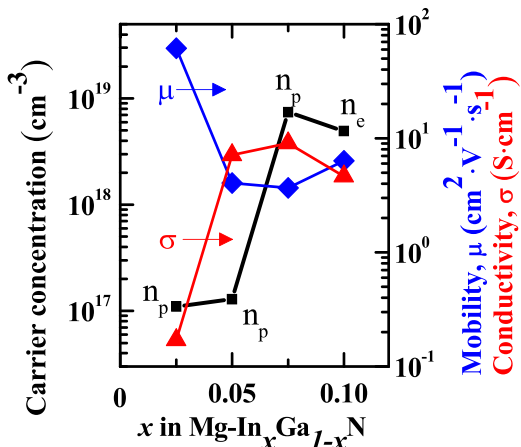


Fig. 4. Electrical properties of carrier concentration, mobility, and electrical conductivity for Mg-In_xGa_{1-x}N films at $x=0.025, 0.05, 0.075$, and 0.1 .

and $7.4 \times 10^{18} \text{ cm}^{-3}$, respectively. The mobility of Mg-In_{0.05}Ga_{0.95}N and Mg-In_{0.075}Ga_{0.925}N films decreased to 4.1 and $3.7 \text{ cm}^2 \text{ V}^{-1} \text{ s}^{-1}$ due to the high hole concentration to increase the carrier scattering.

From the EDS results, the Mg-In_xGa_{1-x}N films were at the nitrogen deficiency state, which can generate the nitrogen vacancies (V_N) as the donor defect to enhance the electron concentration, but these films still has the *p*-type conduction. The strong *p*-type behavior indicates the Mg doping is successful with Mg incorporating into the Ga lattice to act as an acceptor, even though the deposition temperature was only 400°C . We also found that Mg-In_{0.04}Ga_{0.96}N film made by MOVPE showed high holes concentration of $1.2 \times 10^{18} \text{ cm}^{-3}$ [6], this value was close to our result. By our sputtering method, we could obtain the similar electronic quality of the films grown by MOCVD. However, as the In content increased to 16.2% for Mg-In_{0.1}Ga_{0.9}N film, the film transformed into the *n*-type conduction due to the dominance of nitrogen vacancy donor over Mg_{Ga} acceptor. The electron concentration of Mg-In_{0.1}Ga_{0.9}N film decreased slightly to $5.0 \times 10^{18} \text{ cm}^{-3}$ and the mobility increased slightly to $6.3 \text{ cm}^2 \text{ V}^{-1} \text{ s}^{-1}$.

Electrical conductivity of Mg-In_xGa_{1-x}N films depends on carrier concentration and mobility. The Mg-In_{0.075}Ga_{0.925}N film had a highest conductivity of 9.1 Scm^{-1} due to the high hole concentration of $7.4 \times 10^{18} \text{ cm}^{-3}$. As the In content increased to 16.2%, the electrical conductivity dropped to 4.6 Scm^{-1} due to the lower electron concentration of $5.0 \times 10^{18} \text{ cm}^{-3}$. In addition, for Mg-InGaN films deposited by MOCVD, thermal annealing process is needed to break the Mg–H bonding and activate the Mg dopant for improved electrical conductivity [8]. In this work, we did not use the metal organic species and hydrogen atmosphere for depositing the Mg-In_xGa_{1-x}N films, therefore the formation of the Mg–H bonding was avoided.

The UV-vis measurements of Mg-In_xGa_{1-x}N films deposited on the transparent glass substrates were conducted at room temperature (RT). From the UV-vis measurements, the band gap (E_g) of Mg-In_xGa_{1-x}N films could be calculated by using the Tauc equation. It is expressed as [15]

$$(\alpha h\nu)^2 = A(h\nu - E_g) \quad (1)$$

where α is the optical absorption coefficient, A is a constant, $h\nu$ is the incident photon energy, and E_g is the energy band gap of the Mg-In_xGa_{1-x}N films. The band gap can be obtained by plotting the $(\alpha h\nu)^2-h\nu$ curves and followed by extrapolating the linear part of the absorption edge to find the intercept with the energy axis, as shown in Fig. 5. The band gap values were found to be 2.91, 2.88, 2.85, and 2.81 eV for Mg-In_xGa_{1-x}N films at $x=0.025, 0.05, 0.075$,

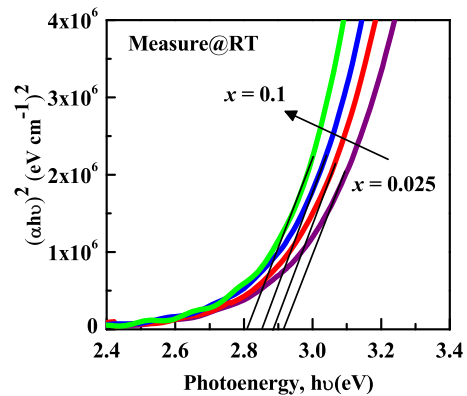


Fig. 5. The $(\alpha h\nu)^2$ versus photon energy ($h\nu$) plot for the optical bandgap determination of the Mg-In_xGa_{1-x}N films at $x=0.025, 0.05, 0.075$, and 0.1 .

0.075, and 0.1, respectively. The slightly red shift ($\Delta E_g=0.11 \text{ eV}$) in the band gap cannot be simply explained by the In content increasing from 5.3 to 16.2% ($\Delta E_g=0.26 \text{ eV}$ in theoretical calculation). The possible explanation can be related to the nitrogen content, which decreases with the increase in the indium content. The more nitrogen vacancies, the more donor levels and the more lattice distortion occur, which can lead to the extended donor levels and make the ΔE_g value unexpectedly lower. Kumakura et al. [6] observed the band gap of Mg-doped In_{0.06}Ga_{0.94}N film deposited by MOVPE to be 2.45 eV. The Mg doping in our In_xGa_{1-x}N did not have an obvious change in E_g because the acceptor level is only 0.1–0.17 eV above the valence band maximum [6].

3.2. *p*–*n* junction diode

p–Mg-In_{0.05}Ga_{0.95}N/*n*-GaN *p*–*n* junction diode was made by RF reactive sputtering on Pt/TiO₂/Si substrate. This device is designed to confirm the *p*-type formation for Mg dopant in In_xGa_{1-x}N (with $x=0.025, 0.05$, and 0.075). The modeling and the cross-sectional profile of *p*–*n* junction diode are shown in Figs. 6 and 7, respectively. By SEM analysis in Fig. 7(a), the thicknesses of Pt and Al layers were found to be $\sim 250 \text{ nm}$. The thicknesses of *n*-GaN and *p*-In_{0.05}Ga_{0.95}N films were measured to be 0.6 and $1.1 \mu\text{m}$, respectively. The microstructure of the *n*-GaN layer had a clear texture structure. On the other hand, the *p*-Mg-In_{0.05}Ga_{0.95}N layer showed a rather random structure. It is expected that the dissolution of Mg and In into the GaN lattice can lead to the lattice distortion and cause the difficulty in the preferential growth. Fig. 7(b) shows the cross-sectional TEM image of the *p*-Mg-In_{0.05}Ga_{0.95}N/*n*-GaN *p*–*n*

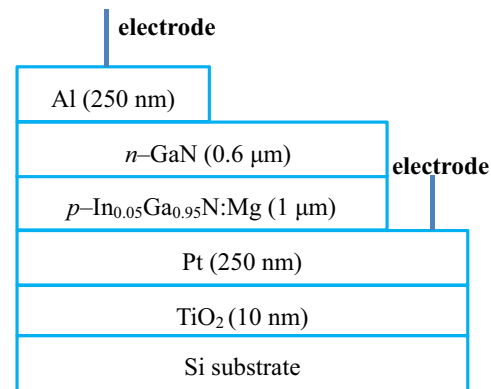


Fig. 6. The structural modeling of a *p*–*n* junction diode.

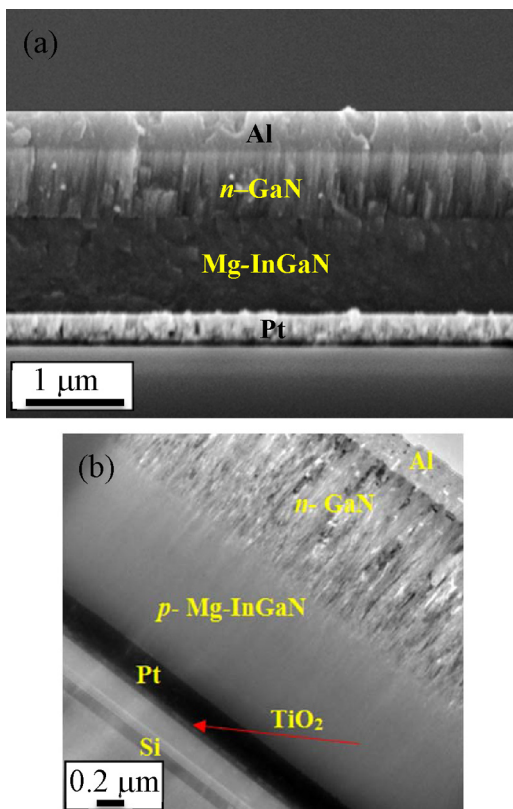


Fig. 7. The cross-sectional (a) SEM and (b) HRTEM images of the $Mg\text{-In}_{0.05}\text{Ga}_{0.95}\text{N}/n\text{-GaN}$ diode.

junction diode. The cross-sectional image in a low magnification gave the image of each layer. Due to the depth difference, the GaN film had showed a clear texture structure.

Fig. 8 shows the current–voltage ($I\text{-}V$) characteristics of diode tested at the room temperature (RT). The leakage current of $p\text{-}n$ junction diode was found to be 2.7×10^{-6} A under the reverse bias of -1 V. From the data in Fig. 8, the turn-on voltage of ~ 1.8 V and the breakdown voltage > -6.8 V were obtained. In addition, the forward and reverse $I\text{-}V$ characteristics of diode were determined at the different temperatures. The semilogarithmic $I\text{-}V$ characteristics of the devices in the temperature range of $25\text{--}150^\circ\text{C}$ are shown in Fig. 9. It is observed that the leakage current at -1 V increases with an increase in temperature from 2.7×10^{-6} to 6.0×10^{-5} A.

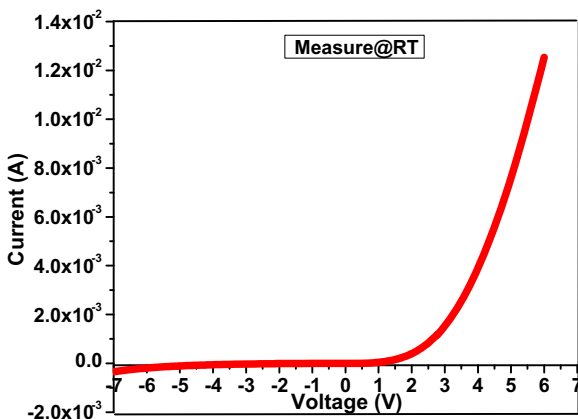


Fig. 8. The $I\text{-}V$ measurement of the $p\text{-}n$ junction diode junction diode measured at the room temperature (RT).

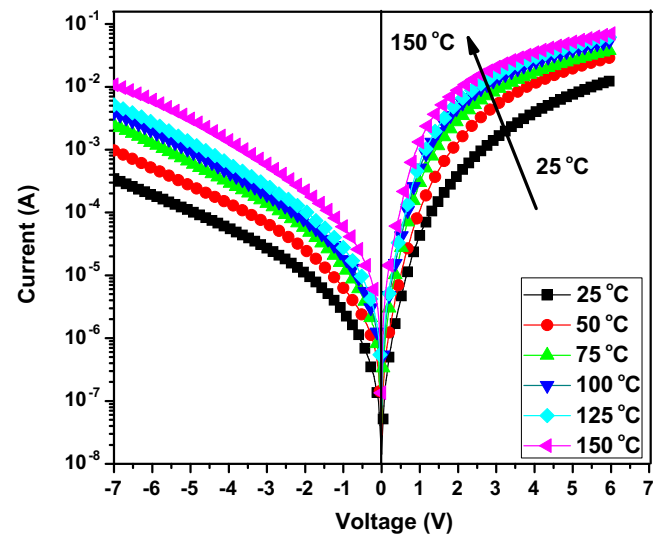


Fig. 9. The semilogarithmic current–voltage ($I\text{-}V$) characteristics of the $p\text{-}n$ junction diode tested at the temperature range of $25\text{--}150^\circ\text{C}$ under the forward and reverse bias.

The electrical characteristics of diodes can be evaluated by using an equation based on the standard thermionic-emission (TE) mode. It can be expressed as below (for $qV > 3kT$) [13,14,16,17]

$$I = I_0 \left[\exp \frac{q}{nkT} (V - IR_s) \right] \quad (2)$$

where V is applied voltage, R_s is the series resistance, n is the ideality factor, and I_0 is the saturation current, q is the electronic charge, T is the experiment temperature in Kelvin, and k is the Boltzmann constant. The plot of $\ln I$ versus V , based upon Eq. (2), can be used to derive the saturation current, which can be obtained by intersecting the interpolated straight lines from the linear region of the semilog plot to zero applied voltage [14,16–18]. Hence, the barrier height of the diode was calculated using the equation [14,19]

$$\phi_B = \frac{kT}{q} \ln \left(\frac{SA * T^2}{I_0} \right) \quad (3)$$

where A^* is the effective Richardson constant and S is the diode area, and ϕ_B the barrier height. In this calculation, the theoretical value of A^* was found to be $26.4 \text{ A cm}^{-2} \text{ K}^{-2}$, based on the effective electron mass ($m^* = 0.22 m_e$) for $n\text{-GaN}$ [14,16,20]. In this study, the area of diode was measured to be 1 mm^2 . In addition, the ideality factor n can be obtained from the slope of the linear region of the forward $I\text{-}V$ characteristics which is determined by the following equation [17–20]

$$n = \frac{q}{kT} \left(\frac{dV}{d(\ln I)} \right) \quad (4)$$

Based upon Eqs. (2)–(4), the barrier height value was found to increase from 0.53 eV at 25°C to 0.66 eV at 150°C , whereas the ideality factor n was found to decrease from ~ 6.1 at 25°C to 3.0 at 150°C .

The effect of series resistance on the electrical properties has been studied using the Cheung's method. The values of series resistance R_s and ideality factor n can be calculated by the following equation [16,19–21]

$$\frac{dV}{d(\ln I)} = \frac{nKT}{q} + IR_s \quad (5)$$

Fig. 10 shows the plot of $dV/d(\ln I)$ versus I (based on Eq. (5)). The linear region is fitted with the linear curve ($y = A + Bx$) and the series resistance R_s and the ideality factor n can be calculated from

Table 2

The parameters calculated from electrical characteristics of a *p-n* junction diode as a function of testing temperature.

Temp (°C)	Leakage current (A) at -1 V	Barrier height ϕ_B (eV)		From <i>I-V</i>	Cheung's function $dV/d(\ln(I))$ versus <i>I</i>	
		<i>I-V</i>	Norde		R_s (Ω)	<i>n</i>
25	2.7×10^{-6}	0.53	0.57	6.1	110	6.3
50	6.3×10^{-6}	0.55	0.60	5.7	60	5.9
75	1.4×10^{-6}	0.59	0.63	4.9	46	5.2
100	2.1×10^{-5}	0.62	0.67	4.4	37	4.7
125	2.7×10^{-5}	0.64	0.71	3.8	34	4.1
150	6.0×10^{-5}	0.66	0.73	3.0	30	3.2

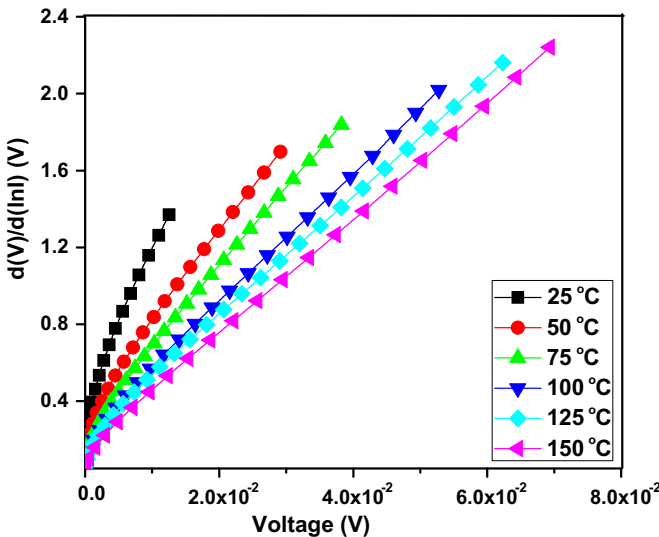


Fig. 10. The $dV/d(\ln(I))$ versus *I* plot for the *p-n* junction diode tested at the temperature range of 25–150 °C.

the intercept and the slope of the straight line [17–21]. The detailed results of the series resistances R_s and ideality factor *n* by the Cheung's method were shown in Table 2.

Norde method was also used to calculate the barrier height of diodes. This method involves a function, $F(V, I)$, plotted versus *V*. The modified Norde function is defined as [17,19,22] (Fig. 11)

$$F(V, I) = \frac{V}{\gamma} - \frac{kT}{q} \ln \left(\frac{I}{AA * T^2} \right) \quad (6)$$

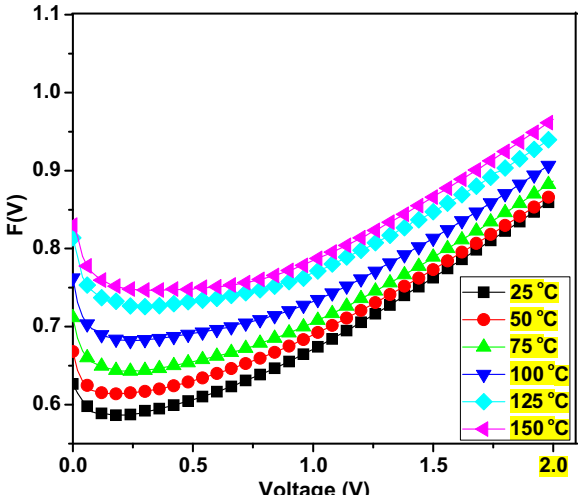


Fig. 11. The $F(V)$ versus *V* plot for the *p-n* junction diode tested at the temperature range of 25–150 °C.

The effective barrier height ϕ_B is followed by

$$\phi_B = F(V_{\min}) + \frac{V_{\min}}{\gamma} - \frac{kT}{q} \quad (7)$$

where γ is the integer (dimensionless) greater than *n*, the $F(V_{\min})$ is the minimum value of $F(V)$, and V_{\min} is the corresponding voltage. Fig. 1 shows the plot of $F(V, I)$ versus *V* as a function of temperature. From the Norde plot, based upon Eqs. (6) and (7), the barrier height value was found to be 0.57 eV at the room temperature and reached 0.73 eV at 150 °C.

Table 2 lists all the derived parameters from the *I-V* measurements of *p-n* junction diode. Under the reverse bias, the lowest leakage current was found at the testing temperature of 25 °C. For the forward bias, the barrier height increased from 0.53 (*I-V*) and 0.57 eV (Norde) at 25 °C to 0.66 (*I-V*) and 0.73 eV (Norde) at 150 °C, respectively. These values of barrier height obtained from the Norde function are in a good agreement compared with the values obtained from *I-V* characteristics. From the data of *I-V* curves and Cheung's method, the extracted ideality factors *n* were in the range of 6.3 (25 °C)–3.0 (150 °C). It is observed that there is a small difference between the values of ideality factor *n* obtained from the $\ln I$ –*V* and $dV/d(\ln I)$ –*I* plot in the forward bias. This difference could be the presence of series resistance, interface states, and the voltage drop across the interfacial layer. There is also a clear trend of decreasing the series resistances R_s with a rise in the testing temperature. The R_s values were observed to drop from 110 Ω at 25 °C to 30 Ω at 150 °C. These achieved parameters for our diode with all layers made by sputtering are consistent with the reported values in some previous papers for *p-n* junction diodes made by other methods [11,13,17,23]. The fall in R_s for films tested at higher temperature indicates that the diode had smaller ideality factor *n*, more free electrons leading to the high current and smaller series resistance in the forward bias. The ideality factor *n* decreased whereas the barrier increased with the increase in the testing temperature. This can be explained that at the room temperature, the flow of the electron transport across the metal-semiconductor interface of devices is able to overcome the lower barriers. Therefore, the current transport will be determined by electrons flowing through the path of lower barrier height and a larger ideality factor. When the testing temperature increases, more and more electrons will have sufficient energy to transcend the higher barrier. As a result, the dominant barrier height will increase with increasing the testing temperature [24,25].

Similar results were also determined by Chen et al. [26]. They studied the current rectification in a single GaN nanowire with a well-defined *p-n* junction. Their ideality factor *n* was calculated in the range of 5.5–6.5. The higher ideality factor was also obtained after testing at lower temperature. Gupta et al. [17] investigated the *p-n* junction based on ZnO and copper phthalocyanine made by pulsed laser deposition and thermal evaporator techniques, respectively. After *I-V* measurement at the room temperature, they reported that the barrier height and ideality factor were 0.63 ± 0.02 eV and 4.0 ± 0.3 , respectively. They also used Cheung's

and Norde methods to calculate and compare for the parameters. Hsueh et al. [27] investigated the temperature dependence of the I - V characteristics of n -Mg_xZn_{1-x}O/ p -GaN hetero junction diodes. They concluded that there was the lowest leakage current at substrate temperature of 25 °C. Furthermore, the extracted ideality factor n was in the range of 3.86–7.00, decreasing with an increase in the testing temperature (25–125 °C). The obtained electrical parameters from our diode made all by sputtering are matched to the previous data for III-nitride devices made by MOCVD.

4. Conclusions

Mg-doped In_xGa_{1-x}N (Mg-In_xGa_{1-x}N) films have been successfully deposited on Si (100), Pt/TiO₂/Si, and glass substrates by RF reactive sputtering at 400 °C with single cermet targets. With $x = 0.025, 0.05$, and 0.075, the Mg-In_xGa_{1-x}N films had the wurtzite structure, good electrical properties, and the p -type conduction without thermal annealing process. The Mg-In_{0.025}Ga_{0.975}N film had the highest mobility of $62 \text{ cm}^2 \text{ V}^{-1} \text{ s}^{-1}$, meanwhile the Mg-In_{0.075}Ga_{0.925}N film had a highest conductivity of 9.1 Scm^{-1} due to the high hole concentration of $7.4 \times 10^{18} \text{ cm}^3$. However, for Mg-In_{0.1}Ga_{0.9}N film (with $x=0.1$), the In content increased to 16.2% even though the In content in the target only 10%. Hence, the excess In caused the film transformed into n -type conduction. Especially, p -In_{0.05}Ga_{0.95}N/ n -GaN junction diode was made successfully by RF reactive sputtering. At room temperature, the leakage current of diode was found to be $2.7 \times 10^{-6} \text{ A}$ under the reverse bias of -1 V . The turn-on and breakdown voltages were also determined to be 1.8 V and $>-6.8 \text{ V}$, respectively. In addition, I - V characteristics of p - n junction diode were tested in the different temperatures. By using equations based on the standard thermionic-emission (TE) mode, Cheung's, and Norde methods, the barrier height increased from 0.53 (I - V) and 0.57 eV (Norde) at 25 °C to 0.66 (I - V) and 0.73 eV (Norde) at 150 °C. The series resistance R_s and ideality factor n decreased from 110Ω to 30Ω and 6.3 to 3.0, respectively, as the testing temperature changed from 25 °C to 125 °C.

Acknowledgment

This work was supported by the Ministry of Science and Technology of Taiwan under grant number 102-2221-E-011-019-MY2.

References

- [1] W.C. Ke, S.R. Jian, I.C. Chen, J.C. Jang, W.K. Chen, J.Y. Juang, Mater. Chem. Phys. 136 (2012) 796–801.
- [2] W. Lee, J. Lim, J.H. Ryou, J. Disp. Technol. 3 (2007) 126–132.
- [3] S.J. Chang, C.H. Chen, P.C. Chang, Y.K. Su, P.C. Chen, Y.D. Jou, H. Hung, S.W. Wang, B.R. Huang, IEEE Trans. Electron Dev. 50 (2003) 2567–2569.
- [4] J.W. Ager, N. Miller, R.E. Jones, K.M. Yu, J. Wu, W.J. Schaff, W. Walukiewicz, Phys. Status Solidi 245 (2008) 873–877.
- [5] G.C. Chi, C.H. Kuo, J.K. Sheu, C.J. Pan, Mater. Sci. Eng. B75 (2000) 210–213.
- [6] K. Kumakura, T. Makimoto, N. Kobayashi, Jpn. J. Appl. Phys. 39 (2000) 337–339.
- [7] C.A. Chang, T.Y. Tang, P.H. Chang, N.C. Chen, C.T. Liang, Jpn. J. Appl. Phys. 46 (2007) 2840–2843.
- [8] K. Sasamoto, T. Hotta, K. Sugita, A.G. Bhuiyan, A. Hashimoto, A. Yamamoto, K. Kinoshita, K.K. Kohji, J. Cryst. Growth 318 (2011) 492–495.
- [9] W. Lee, J. Lim, J.H. Ryou, D.W. Yoo, T. Chung, R.D. Dupuis, J. Cryst. Growth 287 (2006) 577–581.
- [10] J. Cao, J.A. Laroche, F. Ren, S.J. Peaton, J.A. Lothian, R.K. Singh, R.G. Wilson, H.J. Guo, S.J. Pennycook, Solid State Electron. 43 (1999) 1235–1238.
- [11] C.R. Lee, K.W. Seol, J.M. Yeon, D.K. Choi, H.K. Ahn, J. Cryst. Growth 222 (2001) 459–464.
- [12] Y.J. Liu, D.F. Guo, K.Y. Chua, S.Y. Cheng, J.K. Liou, L.Y. Chen, T.H. Tsai, C.C. Huang, T.Y. Chen, C.S. Hsua, T.Y. Tsai, W.C. Liu, Displays 32 (2011) 330–333.
- [13] M.Z. Yusoff, Z. Hassan, N.M. Ahmed, H.A. Hassan, M.J. Abdullah, M. Rashid, Mater. Sci. Semicond. Process. 16 (2012) 1859–1864.
- [14] C.C. Li, D.H. Kuo, J. Mater. Sci.-Mater. Electron. 25 (2014) 1942–1948.
- [15] S. Muthukumaran, R.R. Gopalakrishnan, Opt. Mater. 34 (2012) 1946–1953.
- [16] M. Ravinanda, P.K. Rao, V.R. Reddy, J. Opt. Adv. Mater. 10 (2008) 278–292.
- [17] R.K. Gupta, F. Yakuphanoglu, K. Ghosh, P.K. Kahol, Microelectron. Eng. 88 (2011) 3067–3069.
- [18] R.K. Gupta, K. Ghosh, P.K. Kahol, Physica E 41 (2009) 617–620.
- [19] N.N. Reddy, V.R. Reddy, C.J. Choi, Mater. Chem. Phys. 130 (2011) 1000–1006.
- [20] S.P. Reddy, A.A. Kumar, V.A. Reddy, Thin Solid Films 519 (2011) 3844–3850.
- [21] S. Cheung, N.W. Cheung, Appl. Phys. Lett. 49 (1986) 85–87.
- [22] H.H. Norde, J. Appl. Phys. 50 (1979) 5052–5053.
- [23] D.H. Hwang, S.H. Kang, J.H. Lim, E.J. Yang, J.O. Oh, J.H. Yang, S.J.S.J. Park, Appl. Phys. Lett. 86 (2005) 222101.
- [24] A.A. Kumar, S. Arafat, M.C. Amann, R. Singh, Nanoscale Res. Lett. 8 (2013) 481–488.
- [25] R. Padma, V. Reddy, Adv. Mater. Lett. 1 (2014) 31–38.
- [26] G. Cheng, A. Kolmakov, Y. Zhang, M. Moskovits, R. Munden, M.A. Reed, G. Wang, D. Moses, J. Zhang, Appl. Phys. Lett. 83 (2003) 1578–1580.
- [27] K.P. Hsueh, Microelectron. Eng. 88 (2011) 1016–1018.